5º CONGRESSO BRASILEIRO DE PESQUISA E DESENVOLVIMENTO EM PETRÓLEO E GÁS

TÍTULO DO TRABALHO:

Deslocamento de líquidos em canais com constrições

AUTORES:

Oldrich Joel Romero

INSTITUIÇÃO:

Universidade Federal do Espírito Santo (UFES/CEUNES)

GAS-LIQUID DISPLACEMENT IN CHANNEL WITH CONSTRICTIONS

Abstract

O escoamento de fluidos em meios porosos é um fenômeno bastante complexo. Os caminhos por onde o fluido se desloca é cheio de tortuosidades, obstruções e ocorrem em escala microscópica. Nestas dimensões, o escoamento é governado pela competição das forças viscosas e forças capilares, o quociente destas forças é o parâmetro adimensional chamado número de capilaridade. Quando este adimensional é menor do que 1, a capilaridade criada pela tensão superficial existente na fronteira gás-líquido, ou tensão interfacial no caso da fronteira ser líquido-líquido, governa o escoamento.

Para aumentar o fator de recuperação do petróleo contido nas rochas reservatório, gás ou líquido é bombeado desde a superfície através dos poços injetores. Os fluidos contatados pelo gás ou água escoam ao longo do meio poroso e são elevados até a superfície através dos poços produtores. Na superfície são coletados, submetidos a uma separação primaria e transportados até as refinarias onde os produtos derivados são obtidos.

A compreensão de como a geometria, propriedades dos fluidos e condições operacionais influenciam o escoamento no meio poroso é muito importante para minimizar a quantidade de óleo que fica retido nas paredes das rochas porosas. Neste trabalho, o deslocamento de um líquido por gás em canais com constrições será estudado. A presencia das gargantas, ou obstruções, resulta em um escoamento transiente o qual é governado pelas equações de Navier-Stokes e da continuidade com apropriadas condições iniciais e de contorno. Para simplificar o problema, o fluido é considerado como sendo Newtoniano e o escoamento bi-dimensional. A superfície livre criada pelo contato gás-líquido é descrita utilizando a técnica denominada de geração elíptica da malha, onde a solução de um par de equações escalares permite descobrir a posição de cada nó a cada passo de tempo. O sistema de equações é resolvida em forma acoplada utilizando o método de Galerkin dos elementos finitos. As gargantas são aproximadas por funções senoidais as quais permitem explorar a intensidade da constrição. Resultados iniciais mostram que a superfície livre é muito bem representada e permite observar a bolha invadindo a garganta.

Keywords: Constrições, superfície livre, recuperação, escoamento transiente, Galerkin/FEM.

1. Introduction

Fluids entering the wellbore from the reservoir can range from an undersaturated oil to single-phase gas. Free water can accompany the fluids as a results of water coning, water flooding, or production of intersticial water. Alternative, a free gas saturation in an oil reservoir can result in a gas/liquid mixture entering to the well. Retrograde condensation can result in hydrocarbon liquids condensing in a gas condensate reservoir.

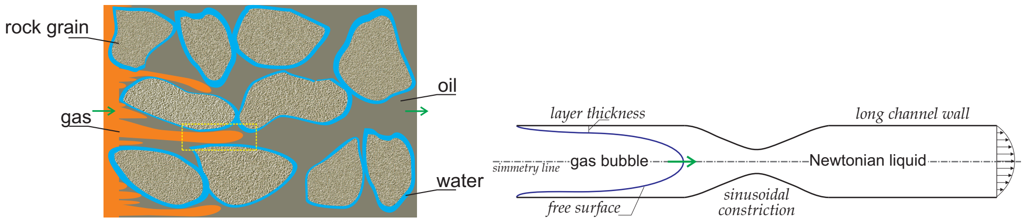

Figure 1: Schematic microscopic representation of the porous media containing oil, gas and connate water. Left side: Sketch of the physical model

The two-phase immiscible flow through oil saturated consolidated porous media is of great practical interest, specially in enhanced oil recovery (Slattery, 1974). There are other practical applications and physical operations where the common basic characteristic is the gas displacing a viscous liquid, such as the monolith reactors, the pulmonary airway reopening, the gas-assisted injection molding. Many authors with quite different approaches have been studied this multifaceted problem.

Immiscible flooding with gas is considered to be one of the most effective enhanced oil recovery processes applicable to light and medium oil reservoirs. Fig. 1 shows a oil being displaced by gas, where the basic interest is the shape of the interface during displacement.

In spite of the importance of the subject, prior studies were mainly related to the gas-liquid displacement in straight tubes and channels, and the gas bubble formed while displacing the liquid was considered semi-infinite, making the motion steady, see for example Taylor (1961), Bretherton (1961), Cox (1962). A few numerical studies have been conducted related with the flow in constricted geometries.

The Taylor bubble problem consist of two fluids: a gas of negligible density in a interior of the bubble and an incompressible Newtonian fluid in the exterior of the bubble. The bubble is symmetric and infinitely long which. Comprehensible reviews on capillary displacements are available in the literature, see for example Olbricht (1996) and Stark and Manga (2000).

Fairbrother and Stubbs (1935) calculated film thickness h from direct measurements of backflow in capillary tubes and established remarkably simple empirical correlation for moving bubbles sufficiently long, i.e. $> 3r$, so that the bubble can be considered cylindrical: $h = (r/2)\sqrt{Ca}$. The dimensional group $Ca = U_b\mu/\sigma$ is the capillary number and represents the relation between the forces increasing distortion of the bubble and hence an increase of h (will increase with bubble velocity U_b and fluid viscosity μ), and the forces resisting distortion (will increase with bubble curvature $1/r$ and surface tension σ), Marquessault and Mason (1960).

The rock pores has been extensively studied approximating the tortuous path as a single straight tube by several researchers Olbricht (1996), Stark and Manga (2000) or in a Helle-Shaw cell. Also, this complex porous media have approximated with a tube of varying cross section for single phase flow. However, studies with two-phase flows in tubes or channels with constrictions are rare. It kind of geometry is appropriated for describe the converging-diverging character of each path of the reservoir.

The objective of the work presented in this paper is to presents a transient numerical simulation of the dynamic of a gas liquid displacement in channels whit constrictions based on the numerical technique presented in Romero and Carvalho (2008). The main focus of this initial research is a study of the influence of the intensity of the channel constriction upon the gas-liquid interface and the obtain a complete picture of the dynamic evolution of the bubble surface and flow field ahead and behind its tip. Because the fluid flow is very slow, around 1 ft/day, is possible to assume that in this approach the inertial terms are negligible when compares with the viscous terms, which means that the Reynolds number (inertial over viscous forces) is zero in our research.

2. Problem formulation

2.1 Governing equations, boundary and initial conditions

Figure 2 shows the domain with a gradually contraction between the upper wall and its symmetry line. At the begin, the domain is completely filled by the Newtonian liquid forming a flat free surface at the entrance of the channel. The liquid is displaced by a pressurized gas from left to right which is increased abruptly from zero to a prescribed value causing a continuous deformation of the free surface, a bubble gas is created which invades the varying slot channel diminishing the volume of liquid. A three-phase contact line is formed in the upper left side corner, we considered this contact line pined to the corner, for a deep discussion about this subject refers to Romero et al. (2006). A film thickness is deposited in the wall.

The governing equations are written in a two-dimensional rectangular coordinates where x and y are the horizontal and vertical co-ordinates, respectively. Because the problem is considered symmetrical, as shown in Fig. 2, only half of the domain is considered, reducing the computational effort dispensed to solve the problem.

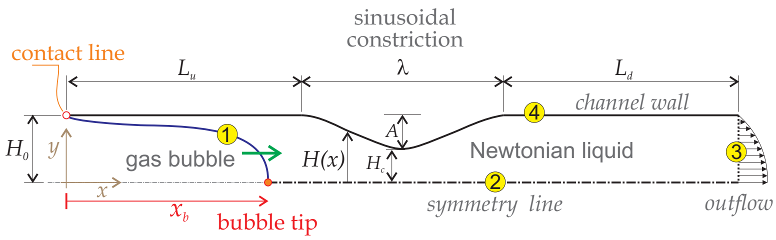

Figure 2: Flow domain and boundary conditions for gas-liquid displacement in a constricted channel.

The gap of the channel varies in the axial direction, x, according to

$$
\begin{aligned}
& = H_0, \qquad 0 \leq x < L_u \\
H(x) & = H_0 - A\,sin(2\pi x/\lambda), \qquad L_u \leq x \leq L_u + \lambda \\
& = H_0, \qquad L_u + \lambda < x \leq L_u + \lambda + L_d,
\end{aligned}
\tag{1}
$$

where A and λ represent the amplitude and wavelength of corrugation, respectively. The planar geometry consists of three parts: an introductory segment of constant gap H_0 and length L_u, a harmonically varying middle part of length λ, and a exit segment of constant gap H_0 and length L_d. The minimum gap is H_c.

The equations governing the transient, two-dimensional, incompressible flow field in the absence of inertial effects (i.e., when Reynolds number $\ll 1$) can be written as

$$\nabla \cdot \mathbf{v} = 0, \tag{2}$$

$$\rho\left(\frac{\partial \mathbf{v}}{\partial t} + \mathbf{v}\cdot\nabla\mathbf{v}\right) - \nabla\cdot\mathbf{T} = 0, \tag{3}$$

where $\mathbf{v} = (u, v)$ and pressure p are the velocity and pressure fields, respectively; ρ is the liquid density. The total stress tensor for Newtonian liquids is $\mathbf{T} = -p\mathbf{I} + \mu[\nabla\mathbf{v} + (\nabla\mathbf{v})^{\mathrm{T}}]$, where μ is the liquid dynamic viscosity and the superscript $^{\mathrm{T}}$ means transpose. Because of the small dimensions of the flow, body forces are usually neglected.

The flow domain and its boundaries are labelled in Fig. 2, the corresponding boundary conditions are:

(1) At the inflow plane, where the gas displaces the liquid, there is a free surface; the velocity field should satisfy a local force balance between the traction in the liquid, the capillary pressure and the gaseous pressure, given by Eq. (4). It is assumed that the gas viscosity is much smaller than the liquid viscosity, leading to vanishing shear stress along the gas-liquid interface

$$\mathbf{n}_{fs}\cdot\mathbf{T} = \sigma\frac{d\mathbf{t}_{fs}}{ds} - \mathbf{n}_{fs}\,P_{in}, \tag{4}$$

where σ is the liquid surface tension, $\mathbf{t}_{fs}$ and $\mathbf{n}_{fs}$ are the local unit tangent and unit normal vectors to the free surface (identified by the subscript $_{fs}$), $d\mathbf{t}_{fs}/ds$ represents the curvature of the meniscus and s the arc-length coordinate along the free surface. P_{in} is the pressure imposed at the free surface located in the entrance of the channel. A step change in this value is applied: at $t = 0$ pressure is suddenly increased to $P_{in} = 3.63$ and remains constant until the end of the computations, this is when the last time t_{LAST} is reached. Also, there is no mass flow rate across the gas-liquid interface, and following Christodoulou and Scriven (1992) we use the kinematic condition considering the mesh velocity $\overset{\circ}{\mathbf{x}}$

$$\mathbf{n}_{fs}\cdot\left(\mathbf{v} - \overset{\circ}{\mathbf{x}}\right) = 0, \tag{5}$$

(2) Along the symmetry line, both the shear stress and the vertical velocity vanish

$$\mathbf{n}\cdot\mathbf{v} = 0, \quad \mathbf{n}\cdot(\mathbf{T}\cdot\mathbf{t}) = 0, \tag{6}$$

$\mathbf{n}$ and $\mathbf{t}$ are the unit vector normal and tangent to the boundary.

(3) At the outflow plane, fully developed parallel rectilinear flow and pressure imposed $P_{out} = 0$ are used

$$\mathbf{n}\cdot(\nabla\mathbf{v}) = 0, \quad p = P_{out}, \tag{7}$$

the outflow plane was located at a distance equal to $5H_0$ downstream from the constriction. Changes on its location did not affect the steady state solution.

(4) The no-slip and no-penetration conditions applies along the channel walls

$$u = 0, \quad v = 0. \tag{8}$$

Finally, an initial condition is needed in order to solve the transient flow problem. In this work, we assume the initially there is no flow and the pressure field is uniform in all the domain

$$\mathbf{v}(t=0)=\mathbf{0}, \quad p(t=0)=0. \tag{9}$$

The operating parameters can be grouped in the following dimensionless parameters:
(i) Capillary number $Ca \equiv \mu V_w/\sigma$, which measures the ratio of viscous stress to pressure generated by surface tension in curved meniscus.
(ii) Reynolds number $Re \equiv \rho V_w H_0/\mu$, which measures the ratio of inertial to viscous forces.

2.2 Geometries

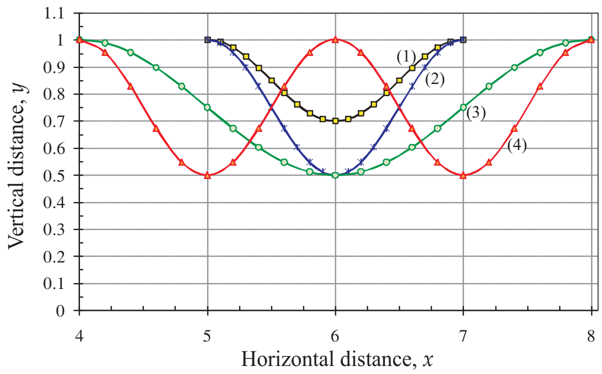

Figure 3: Configurations of the channel constriction.

The transient, two-dimensional flow in the Helle-Shaw cell was analyzed at different amplitudes and frequencies of the imposed oscillation. In order to explore the effect of the geometry of the constriction, four different wall configurations were considered; they are shown in Fig. 3. The feed slot height $H_f = H_0$ and the downstream die lip length $L = 6H_0$ were the same in all configurations. In the base geometry, Fig. **??**-a, the upstream and downstream gap were equals, e.g. $H_d = H_u = H_0$. The other two configurations consisted of what is called underbite and overbite setups. In the first, the upstream gap is larger than the downstream gap, $H_u = 1.4H_0$ and $H_d = H_0$. In the latter, the upstream gap is smaller than the downstream gap, $H_u = 0.6H_0$ and $H_d = H_0$. In all cases analyzed here, the vacuum pressure was set such that the steady state location of the upstream meniscus was at $x_{dyn} \approx 6H_0$. In all different configurations, the downstream gap is set at $H_d = H_0 =$100 μm.

3. Solution method

3.1 Formulation of the free boundary problem

The primary difficulty in applying the finite element method (FEM) to free-surface problems is the need to specify a procedure for constructing a mesh over the domain, the shape of which is *a priori* unknown. For those FEM problems which involve free surfaces that move during the computation, an initial mesh can be updated simply by using a continuous deformation algorithm which maintains the same mesh connectivity throughout the problem. In preserving connectivity, we also preserve the sparsity patterns of the various matrices that arise in the discretisation solution of the problem, e.g. stiffness and mass matrices, Jacobians, etc., with obvious efficiency advantages.

The shape of the interface needs to be determined as part of the solution. Several schemes for obtaining the shape of the free surface together with the velocity and pressure fields are available.

In our work, in order to solve this free boundary problem by means of standard techniques for boundary value problems, the set of differential equations and boundary conditions posed in the unknown domain had to be transformed to an equivalent set defined in a known reference domain. This transformation was made by a mapping $\mathbf{x} = \mathbf{x}(\xi)$ that connects the two domains. The unknown physical domain was parameterized by the position vector $\mathbf{x}$, and the reference domain by $\boldsymbol{\xi}$. The mapping used here was the one described by de Santos (1991). The inverse of the mapping that minimizes the functional is governed by a pair of elliptic differential equations identical to those encountered in diffusional transport with variable diffusion coefficients. The coordinates potentials ξ and η of the reference domain satisfied

$$\nabla \cdot (D_\xi \nabla \xi) = 0 \qquad ; \qquad \nabla \cdot (D_\eta \nabla \eta) = 0. \tag{10}$$

D_ξ and D_η are diffusion-like coefficients used to control gradients in coordinate potentials, and thereby the spacing between curves of constant ξ on the one hand and of constant η on the other that make up the sides of the elements that were employed; they were quadrilateral elements. Boundary conditions were needed in order to solve the second-order partial differential equations Eqs. (10). The solid walls and synthetic inlet and outlet planes were described by functions of the coordinates and along them stretching functions were used to distribute the terminii of the coordinate curves selected to serve as element sides. The free boundary (gas-liquid interface) required enlarging the system of governing equations with the kinematic condition, viz. Eq. (5). The discrete version of the mapping equations is generally referred to as mesh generation equations.

In transient problems the frame of reference lies across the space-time domain for which the physical grid points are constantly updated in time. Therefore, time derivative at fixed Eulerian locations in space $\partial\Psi/\partial t$ needs to be transformed to time derivative at fixed iso-parametric coordinates, denoted by $\overset{\circ}{\Psi}$. As described by Christodoulou and Scriven (1992), the following transformation is employed

$$\frac{\partial \Psi}{\partial t} = \overset{\circ}{\Psi} - \overset{\circ}{\mathbf{x}} \cdot \nabla \Psi, \tag{11}$$

where $\overset{\circ}{\mathbf{x}}$ is the mesh velocity, the time derivative of the nodal position.

Using Eq. (11) for the local velocity time derivative $\partial\mathbf{v}/\partial t$ in Eq. (3), the momentum equation becomes

$$\rho \left[\overset{\circ}{\mathbf{v}} + (\mathbf{v} - \overset{\circ}{\mathbf{x}}) \cdot \nabla \mathbf{v} \right] - \nabla \cdot \mathbf{T} = 0. \tag{12}$$

3.2 Spatial discretization by Galerkin / finite element method

The system of governing equations, Eqs. (12), (2) and (10), together with the appropriate boundary conditions was solved by Galerkin's method with quadrilateral finite elements.

The weighted residual equations are obtained after multiplying each governing equation by weighting functions $\varphi^{\mathbf{m}}$, φ^{c}, and $\varphi^{\mathbf{x}}$, integrating over the unknown flow domain Ω (bounded by Γ), applying the divergence theorem to the terms with divergences and mapping the integrals onto the known reference domain $\overline{\Omega}$ (bounded by $\overline{\Gamma}$). In Galerkin's method, the weighting and the basis functions are the same. Superscript $^{\mathbf{m}}$, ^{c}, and $^{\mathbf{x}}$ denotes momentum, continuity, and mesh residuals.

Each independent variable $\mathbf{v}$, p and $\mathbf{x}$ is approximated with a linear combination of a finite number of known basis functions $\varphi_j^{\mathbf{v},p,\mathbf{x}}(\xi,\eta)$

$$\mathbf{v} = \sum_j^M \widetilde{\mathbf{v}}_j(t)\,\varphi_j^{\mathbf{v}}(\xi,\eta), \quad p = \sum_j^N \widetilde{p}_j(t)\,\varphi_j^{p}(\xi,\eta), \quad \mathbf{x} = \sum_j^M \widetilde{\mathbf{x}}_j(t)\,\varphi_j^{\mathbf{x}}(\xi,\eta); \tag{13}$$

$\widetilde{\mathbf{v}}_j(t)$, $\widetilde{p}_j(t)$ and $\widetilde{\mathbf{x}}_j(t)$, are the basis functions coefficients, and represents the unknowns of the discretized problem; they are arranged in a vector of basis function coefficients:

$$\mathbf{u}(t) \equiv [\widetilde{\mathbf{v}}_j(t), \widetilde{p}_j(t), \widetilde{\mathbf{x}}_j(t)]^{\mathrm{T}}. \tag{14}$$

The velocity and node positions were represented in terms of Langrangian biquadratic basis functions $\varphi_j^{\mathbf{v}}(\xi,\eta) = \varphi_j^{\mathbf{x}}(\xi,\eta)$, and the pressure in terms of linear discontinuous basis functions $\varphi_j^{p}(\xi,\eta)$. This is the so called mixed formulation, higher order polynomials to interpolate the velocity field than the pressure, and the combination is appropriate for avoid instabilities during the process solution for Newtonian liquids; also know as the Babuska-Brezzi condition (Fortin, 1981).

Once all the variables are represented in terms of the basis functions, the system of partial differential equations reduces to a set of ordinary differential and algebraic equations that describe the evolution of the coefficients with time:

$$\mathbf{R}(\mathbf{u}, \dot{\mathbf{u}}, \mathbf{f}) = 0, \tag{15}$$

where $\mathbf{R}$ is the set of weighted residual equations, $\mathbf{u}$ is the vector of basis functions' coefficients, $\dot{\mathbf{u}}$ is their time derivatives, and $\mathbf{f}$ a vector that contain all the input parameters (physical properties, geometry of the flow and boundary condition information).

Additional details of this derivation we refer to Romero and Carvalho (2008) where is presented a numerical study of coating flows under periodic disturbances.

3.3 Temporal discretization of the transient equations

The temporal discretization of the set of ordinary differential-algebraic equations, eq. (15), followed a predictor-corrector algorithm. The predictor step consists of a forward Euler method and the corrector step consists of a first-order fully implicit Euler method, which is unconditionally stable. The approximate form of the velocity time-derivatives in the momentum conservation equation, eq. (12), using backward finite difference is

$$\overset{\circ}{\mathbf{v}} \equiv \frac{\mathbf{v}_{n+1} - \mathbf{v}_n}{t_{n+1} - t_n} = f(\mathbf{v}_{n+1}, t_{n+1}), \tag{16}$$

where the indices $n+1$ and n indicates current and previous time instant, respectively. The difference $t_{n+1} - t_n$ defines the current time step Δt_{n+1}. A similar expression is used for the mesh velocity $\overset{\circ}{\mathbf{x}}$.

The system of ordinary differential-algebraic equations (DAEs) is reduced to simultaneous algebraic nonlinear equations for the coefficients of the basis functions of all the fields. At each time step, the resulting set of nonlinear algebraic equations was solved simultaneously by

Newton's method with an initial estimate resulting from an explicit Euler step from the solution at the previous two time steps

$$\left(\frac{1}{\Delta t}\mathbf{M}(\mathbf{u}_{n+1}^{(k)}) + \mathbf{J}(\mathbf{u}_{n+1}^{(k)})\right)\,\delta\mathbf{u}^{(k+1)} = -\mathbf{R}(\mathbf{u}_{n+1}^{(k)}, \mathbf{u}_n), \tag{17}$$

$$\mathbf{u}_{n+1}^{(k+1)} = \mathbf{u}_{n+1}^{(k)} + \delta\mathbf{u}^{(k+1)}; \tag{18}$$

the indices $k+1$ and k indicates the current and previous Newton's step. The iteration is repeated until convergence. Here $\mathbf{J} \equiv \partial\mathbf{R}/\partial\mathbf{u}$ is the Jacobian matrix which measure the sensitivity of the residuals to the unknowns of the problem, the entries of this matrix are calculated analytically; and $\mathbf{M} \equiv \partial\mathbf{R}/\partial\dot{\mathbf{u}}$ is the mass matrix which measure the sensitivity of the residuals to changes in the time derivatives of the unknowns. Because the finite element basis functions used are different from zero only over a very small portion of the domain, the Jacobian matrix is sparse and was stored in compressed sparse formats. In each Newton's iteration, the linearized form of Eq. (17) was factorized into a lower $\mathbf{L}$ and upper $\mathbf{U}$ triangular matrix by the frontal solver (Almeida, 1996).

The tolerance on the L2-norm of the residual vector and on the last Newton update of each declared solution was set to 10^{-6}. The sensitivity of the computed solution to the size of the time step used was tested by comparing the transient response obtained with different time steps. The solution varied by less than 2% if the time step Δt was smaller than 1.5.

A mesh convergence analysis was done by comparing the free surface configuration at capillary number $Ca = 0.2$, with three different meshes. A mesh with 680 elements (13.356 degrees of freedom) was considered satisfactory and was used to obtain the solutions reported here. Further refining this mesh, led to changes on the bubble tip position of less than 1 $\%$.

4. Results and discussion

The Newtonian liquid initially occupies the entire domain. At the beginning of the computations $t = 0$ the gas-liquid interface is considered flat. A step change in the pressure P_{in} is applied on the gas side of the gas-liquid interface at the entrance of the channel throughout the Eq. (4) forcing the transient penetration of the gas bubble into the varying slot crated by the neck in the parallel plates. Because of that, the steady state is not reached and the flow domain changes in shape and size, demanding a reconstruction of the mesh several times. Differently from another approaches –Fairbrother and Stubbs (1935), Fairbrother and Stubbs (1935), Fairbrother and Stubbs (1935)– where the wall is and the bubble is static, in our work the wall is fixed. Because the prescribed pressure at the exit of the domain is $P_{out} = 0$, the applied pressure difference remains constant. But, once the bubble moves along the slot in direction to the output boundary, the volume of the liquid in the domain decrease reducing the resistance to the flow. This results in an acceleration of the flow field.

Computations are performed until $t = t_{LAST}$ has been reached. The last time, t_{LAST}, is different for each geometry because the mesh deformation limits is influenced by the type of constriction present in the channel.

A gas bubble moving at constant pressure through a constricted noncircular capillary is illustrated in Fig. 4. As the bubble invades the constriction, the mean curvature of the gas-liquid interface increases, so that the bubble front may squeeze into the constriction. After the front has passed the tightest part, or neck, of the constriction, the interfacial curvature begins to decrease. As commented by Ransohoff et al. (1987) "this drop in curvature, if sufficiently

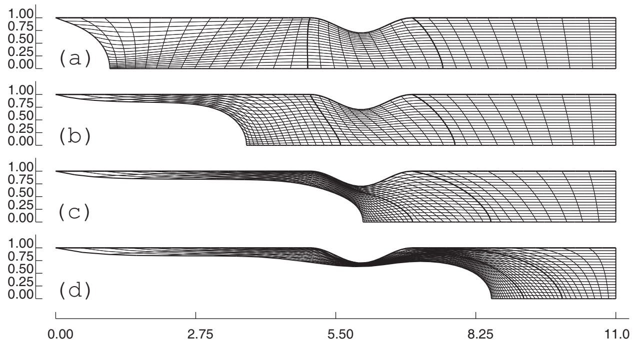

Figure 4: Mesh bubble evolution at different time instants as a function of the time step Δt: (a) $12\Delta t$, (b) $48\Delta t$, (c) $71\Delta t$ and (d) $86\Delta t$. The geometry for this case is the number (1) showed in Fig. 3

large, initiates a wetting-liquid pressure gradient directed from the front of the bubble to the neck of the constriction. Liquid flows into the constriction, and eventually enough liquid may accumulate at the constriction neck to block the pore and snap-off a gas bubble". Snap-off occurs when wetting fluid (liquid) accumulates by capillary action in a pore throat occupied by non-wetting phase (gas) and then bridges across the throat to block flow. Capillary pressure must be high enough for gas to invade the throat, but then fall by about a factor of two for liquid to re-invade the throat, which means that if the pore body radius is at least about twice the throat radius, snap-off occurs in agree with the basic Roof's criteria, (Rossen, 2000).

A comparison of bubble position at the last time of computation for the different channel undulation are shown in Fig. 5. In the four cases, the mesh is strongly deformed around the constricted section and when it passes through the constriction. Convergence of the solution process is lost at time instants which are functions of the intensity of the channel variation. The remaining film has a nonuniform thickness distribution being thicker before contractions.

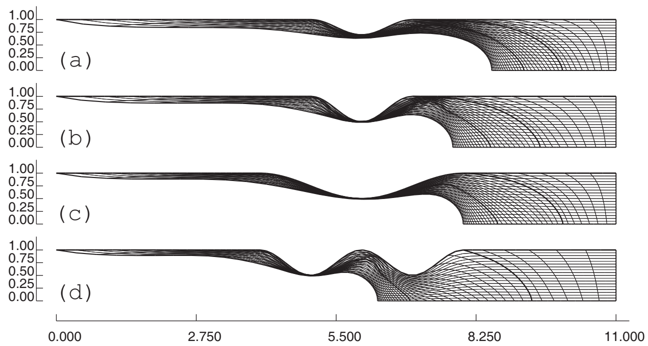

Figure 5: Comparison of the mesh deformation at the last time of computing: (a) $86\Delta t$, (b) $115\Delta t$, (c) $146\Delta t$ and (d) $150\Delta t$; for geometries (1), (2), (3) and (4) respectively.

Fig. 6 shows the time evolution of the bubble tip position for the four channel configurations. The bubble tip moves toward the channel exit monotonically. The evolution of the tip exhibits small-amplitude oscillations. The time required for the bubble tip to reach a certain position in the tube increases with the intensity of the undulation variation.

A strong decline of the pressure of the bubble tip is observed at the beginning of the process, as shown in Fig. 7, after that it declines linearly until it arrives close to the constricted section where pressure decrease is stronger, since more energy is consumed there. In addition, there is a time delay in the response of the pressure at the bubble tip, it has a minimum after the

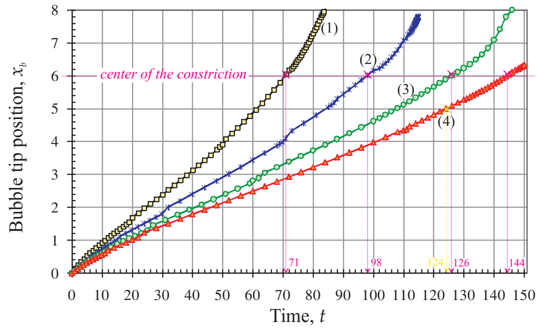

Figure 6: Evolution of the bubble tip position.

bubble front has passed through the channel minimum. For example, the bubble reaches the constriction at $t = 71\Delta t$, and the pressure is minimized at $t = 75\Delta t$. The response of the bubble tip velocity is also presented. The bubble tip velocity is almost constant before the constriction, after the bubble past the constriction, it immediately expands accelerating.

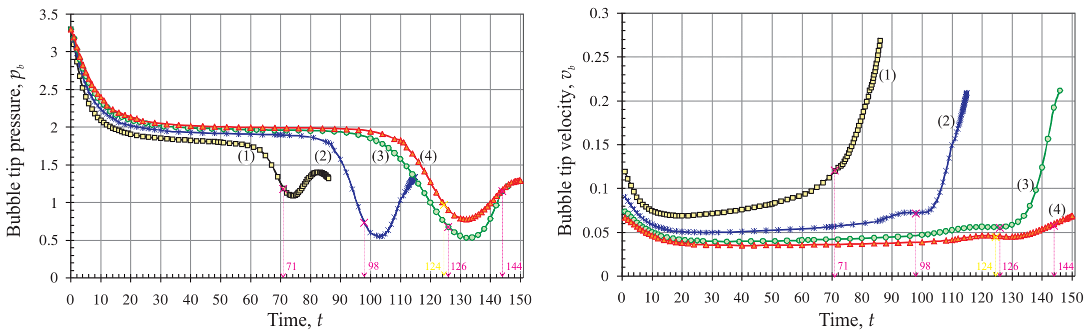

Figure 7: Pressure and velocity of the bubble tip.

5. FINAL REMARKS

Our intention in this work has been to present the numerical technique and the first results obtained when applied to the transient gas-liquid displacement. Certainly is necessary to improve the treatment of this results, especially its presentation using dimensionless parameters. This will be done in the future, when a more refined mesh and a smaller time step will be selected, and running each case in a more powerful computer.

REFERENCES

Almeida, V. F., 1996. *Gas-Liquid counterflow through constricted passages*. PhD thesis, University of Minnesota, MN, USA.

Bretherton, F. P., 1961. The motion of long bubbles in tubes. *J. Fluid Mech.*, vol. 10, pp. 166–188.

Christodoulou, K. N. & Scriven, L. E., 1992. Discretization of free surface flows and other moving boundary problems. *Journal of Computational Physics*, vol. 99, pp. 39–55.

Cox, B. G., 1962. On driving a viscous fluid out of a tube. *J. Fluid Mech.*, vol. 14, pp. 81–96.

de Santos, J. M., 1991. *Two-phase cocurrent downflow through constricted passages*. PhD thesis, University of Minnesota, MN, USA.

Fairbrother, F. & Stubbs, A., 1935. Studies in electroendosmosis. part vi. the bubble-tube methods of measurement. *J. Chem. Soc.*, vol. 1, pp. 527529.

Fortin, M., 1981. Old and new finite elements for incompressible flows. *Int. J. Numer. Methods Fluids*, vol. 1, pp. 347–355.

Marquessault, R. N. & Mason, S. G., 1960. Flow of entrapped bubbles through a capillary. *Ind. and Engineering Chem.*, vol. 52, n. 1, pp. 79–84.

Olbricht, W. L., 1996. Pore-scale prototypes of multiphase flw in porous media. *Annu. Rev. Fluid Mech.*, vol. 28, pp. 187–213.

Ransohoff, T. C., Gauglitz, P. C., & Radke, C. J., 1987. Snap-off of gas bubbles in smoothly constricted noncircular capillaries. *AIChE J.*, vol. 33, n. 5, pp. 753–765.

Romero, O. J. & Carvalho, M. S., 2008. Response of slot coating flows to periodic disturbances. *Chemical Engineering Science*, vol. 63, n. 8, pp. 2161–2173.

Romero, O. J., Scriven, L. E., & Carvalho, M. S., 2006. Effect of curvature of coating die edges on the pinning of contact line. *AIChE J.*, vol. 52, pp. 447–455.

Rossen, W. R., 2000. Snap-off in constricted tubes and porous media. *Colloids and Surfaces A*, vol. 166, pp. 101–107.

Slattery, J. C., 1974. Interfacial effects in the entrapment and the displacement of residual oil. *AIChE J.*, vol. 20, pp. 1145–1154.

Stark, J. & Manga, M., 2000. The motion of long bubbles in a network of tubes. *Transport Porous Media*, vol. 40, pp. 201–218.

Taylor, G., 1961. Deposition of a viscous fluid on the wall of a tube. *J. Fluid Mech.*, vol. 10, pp. 161–165.